Editors' Suggestion | Featured in Physics

Angle Locking of a Levitating Diamond Using Spin Diamagnetism

M. Perdriat, P. Huillery, C. Pellet-Mary, and G. Hétet
Laboratoire De Physique de l'École Normale Supérieure, École Normale Supérieure, PSL Research University, CNRS, Sorbonne Université, Université de Paris, 24 rue Lhomond, 75231 Paris Cedex 05, France

(Received 20 October 2021; accepted 14 February 2022; published 18 March 2022)

Nanodiamonds with embedded nitrogen-vacancy (NV) centers have emerged as promising magnetic field sensors, as hyperpolarizing agents in biological environments, as well as efficient tools for spin mechanics with levitating particles. These applications currently suffer from random environmental interactions with the diamond which implies poor control of the N-V direction. Here, we predict and report on a strong diamagnetism of a pure spin origin mediated by a population inversion close to a level crossing in the NV center electronic ground state. We show control of the sign of the magnetic susceptibility as well as angle locking of the crystalline axis of a microdiamond along an external magnetic field, with bright perspectives for these applications.

DOI: 10.1103/PhysRevLett.128.117203

The electronic spin of the negatively charged nitrogen-vacancy (NV) in diamond has been employed in a broad range of research directions over the past two decades with impressive demonstrations in nanoscale magnetometry [1], and in quantum communication and computing [2]. In the employed platforms, high quality diamonds are typically tethered to a scanning tip for imaging fields above magnetic materials or to a cold finger for minimizing phonon-induced relaxation in coherent spin manipulations. Conversely, major other applications involving the electronic spin of the NV center require diamonds to be untethered. In particular, freely moving or loosely bound nanodiamonds containing NV centers can serve as *in vivo* hyperpolarizing agents in nuclear magnetic resonance [3–6] or as nanomagnetometers in living cells [7]. Another example is spin mechanics with levitating particles [8]. There, single NV centers are envisioned as a bus for creating quantum superpositions of the diamond motion. The underlying idea is that quantum superpositions of the NV electronic spin states can be transferred to the diamond center of mass motion using magnetic field gradients [9] or to the angle using homogeneous B fields [10], which offers perspectives for matter-wave interferometry and tests of quantum gravity [11–14].

When operated in a liquid or trapped under vacuum however, the orientation of the nanodiamonds are subjected to various conservative or viscous forces [15–18]. The spin direction thus changes over time, making it difficult to make full use of its capabilities for sensing and coherent control. One major concern is the lack of NV polarization when the external magnetic field is not along the diamond $\langle 111 \rangle$ axis [19] and the required control over the microwave frequency to adapt for the changing B field projection over the NV axis. Here, we show that NV-doped diamonds behave as materials with strong magnetic anisotropy and can be turned into diamagnets with a large susceptibility. Further, we exploit the spin-diamagnetism to stabilize the $\langle 111 \rangle$ crystalline axes of levitating microdiamonds along the applied magnetic field.

To understand the origin of the NV-doped diamond magnetism, let us first consider a generic nonmagnetic crystal hosting independent atomic defects with unpaired electrons. The dominant magnetization of such a crystal is typically quantified through the variation in the electronic energy levels ϵ_k of the defects as a function of an applied magnetic field $\boldsymbol{B}$ via the formula

$$M_i^S = -d \sum_k \frac{\partial \epsilon_k}{\partial B_i} p_k, \tag{1}$$

where d is the density of the defects, B_i is the magnetic field component along the i direction, and p_k is the population in the state k. This formula, derived using statistical physics principles, is valid when mixed states are involved. Note that we also neglect the demagnetizing field from the defects, which is much smaller than the applied field in typical dilute spin ensembles. The components $\chi_{ij} = \mu_0(\partial M_i^S/\partial B_j)$ of the magnetic susceptibility tensor $\underline{\underline{\chi}}$ then read

$$\chi_{ij} = -d\mu_0 \left[\sum_k \frac{\partial \epsilon_k}{\partial B_i} \frac{\partial p_k}{\partial B_j} + \sum_k \frac{\partial^2 \epsilon_k}{\partial B_i \partial B_j} p_k \right]. \tag{2}$$

The first term in this equation is positive, strongly temperature dependent and gives rise to Langevin paramagnetism. The second term typically has two opposing contributions: a negative contribution coming from the orbital electron motion, namely, the Larmor diamagnetism, and a positive Van Vleck paramagnetic contribution [20,21]. As we will

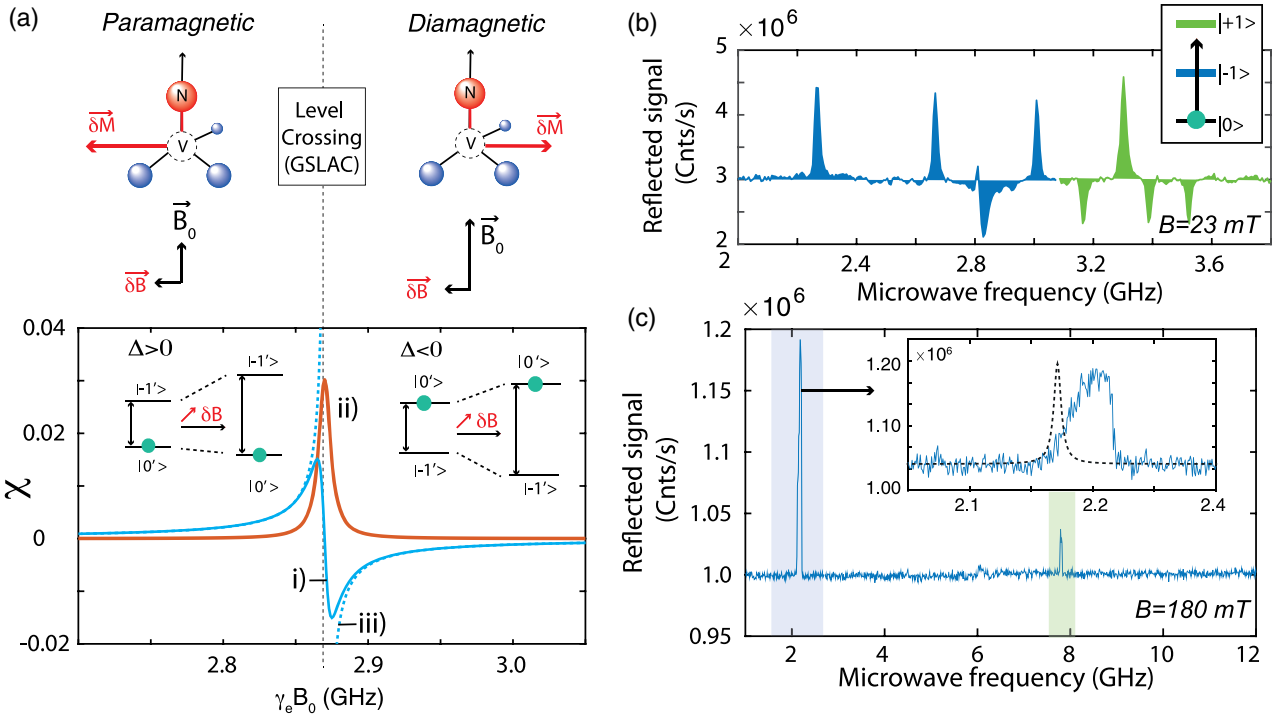

FIG. 1. (a) Trace (i) and trace (ii), show the expected NV susceptibility coefficients $\chi_\perp$ and χ_d as a function of $\gamma_e B_0$. Trace (iii) (in dashed lines) displays $\chi_\perp$ obtained from Eq. (1). The states $|m_s = 0'\rangle$ and $|m_s = -1'\rangle$ are eigenstates of the Hamiltonian away from the level crossing. (b) and (c) Mechanically detected-magnetic resonances measured in the paramagnetic and diamagnetic regime where $B = 23$ and 180 mT, respectively. The inset of (c) is an enlargement on the first spin resonance at 2.2 GHz. The dashed line is a sketch of an MDMR in the weak microwave drive limit (arbitrary scale of the y axis).

show, close to a level crossing, NV-doped diamonds in fact exhibit strong Van Vleck magnetism with a tunable susceptibility.

The ground electronic state of the NV$^-$ center is a triplet state with a zero-field splitting D coming from magnetic dipole-dipole interaction between two unpaired electrons [22]. This interaction sets a natural quantization axis z along the N-V direction shown in Fig. 1(a). One feature of the electronic spin of the NV$^-$ center is that it can be optically polarized to the $|m_s = 0\rangle$ state using green laser light. In the absence of magnetic field, the other $|m_s = \pm 1\rangle$ states both lie $D \approx (2\pi)2.87$ GHz above the $|m_s = 0\rangle$ state at room temperature. In the presence of a magnetic field $\boldsymbol{B}_0$ aligned with the NV axis, the Hamiltonian of the NV$^-$ center electronic spin reads

$$\hat{\mathcal{H}}_0 = \hbar D \hat{S}_z^2 + \hbar \gamma_e B_0 \hat{S}_z, \tag{3}$$

where γ_e is the electron gyromagnetic ratio. In this magnetic field configuration, there is no induced magnetization of the NV-doped diamond because the two magnetic eigenstates $|m_s = \pm 1\rangle$ are equally populated.

As is the case with several paramagnetic crystals [20,23,24], the essence of the presented NV magnetization lies in the state mixing induced by a static magnetic field perturbation $\delta B_\perp$ that is perpendicular to the quantization axes defined by the crystal field. The mixing between the $|m_s = 0\rangle$ and $|m_s = \pm 1\rangle$ states generates a magnetic moment that is perpendicular to the NV axis. Adding a static perturbation $\boldsymbol{\delta B}$, the Hamiltonian becomes $\hat{\mathcal{H}} = \hat{\mathcal{H}}_0 + \hat{V}$, where $\hat{V} = \hbar \gamma_e \boldsymbol{\delta B} \cdot \hat{\boldsymbol{S}}$. Close to level crossings, coherences between eigenstates may no longer be negligible, so the general formula $M_i^{\mathrm{Q}} = -d\hbar\gamma_e \langle \hat{S}_i \rangle$ must be employed instead of Eq. (1), to calculate the magnetization.

One finds that the NV$^-$ center acquires a magnetization $\boldsymbol{\delta M^Q} = \underline{\underline{\chi}}^{\mathrm{NV}} \boldsymbol{\delta B}/\mu_0$ as depicted in Fig. 1(a). The tensor $\underline{\underline{\chi}}^{\mathrm{NV}}$ is rotationally invariant along the $\boldsymbol{e}_z$ axis so its only nonzero components are $\chi_\perp = \chi_{x,x} = \chi_{y,y}$ and $\chi_d = \chi_{y,x} = -\chi_{x,y}$ (see Sec. I of the Supplemental Material [25]). To quantify the nonzero elements of $\underline{\underline{\chi}}^{\mathrm{NV}}$, we first consider a single NV center orientation out of the four [111] directions for simplicity. We also consider a density $d = N/V \approx 1$ ppm and an optical pumping rate γ_{las} to the $|m_s = 0\rangle$ state that is far greater than the longitudinal spin relaxation rate $T_1 \approx 500$ μs [29]. $\chi_\perp$ and χ_d are plotted in Fig. 1(a). We also plot the result of the calculation assuming a statistical mixture of the NV states in trace (iii). In the limit where $\gamma_e B_0 \ll D, \chi_\perp \approx d\hbar\mu_0 2\gamma_e^2/D \approx 10^{-4} > 0$ so that the NV-doped diamond is strongly paramagnetic. Including the four NV centers orientations along the four [111] diamond crystalline axes now, the total susceptibility

drops to about 10^{-5}. This is comparable to the diamond orbital diamagnetism ($\chi_{\mathrm{orb}} \approx 10^{-5}$) [29], which is negligible in our experimental conditions. Close to the ground state level anticrossing (GSLAC) however, the states $|m_s = 0\rangle$ and $|m_s = -1\rangle$ mix much more (see Sec. I-D of the Supplemental Material [25]). In this regime, one finds

$$\chi_\perp \approx d\hbar\mu_0 \frac{\gamma_e^2 \Delta}{\Delta^2 + (\Gamma_2^*)^2}, \tag{4}$$

where $\Delta = D - \gamma_e B_0$ and $\Gamma_2^*/2\pi = 1/T_2^* \approx 5$ MHz is the spin dephasing rate due to the fluctuating dipolar coupling to substitutional nitrogen atoms.

As expected, the formula for $\chi_\perp$ and χ_d only depart from the trace (iii) at the GSLAC. When slightly detuned from resonance, in the so-called dispersive limit $|\Delta| > \Gamma_2^*$, we can interpret the NV^- induced magnetization in terms of Van Vleck magnetism (see Sec. I of the Supplemental Material [25]). Importantly, the maximum susceptibility $|\chi_\perp| \approx 10^{-2}$ is 2 orders of magnitude larger close to the GSLAC than far off-resonance. Further, when $\Delta < 0$, the NV spin population is in the first excited state [see inset of Fig. 1(a)]. The NV intersystem crossing in the optically excited state ^3E indeed preserves polarization in the $|m_s \approx 0\rangle$ state even after the GSLAC, which results in a population inversion, as in the recently demonstrated diamond maser [30]. The possibility to swap populations between $|m_s \approx 0\rangle$ and $|m_s \approx -1\rangle$ states using Δ thus results in a tunable magnetization that can be opposed to (as in a diamagnet) or aligned with (as in a paramagnet) the applied magnetic field perturbation.

One way to determine the magnetization $\boldsymbol{M}$ of a material is to measure the magnetic torque $\boldsymbol{\tau} = V\boldsymbol{M}(\boldsymbol{B}) \times \boldsymbol{B}$ applied to it under an external magnetic field $\boldsymbol{B}$. For NV^- centers at a small angle θ with respect to $\boldsymbol{B}$, we can write $\boldsymbol{B} \approx B_0\boldsymbol{e_z} + \theta B_0\boldsymbol{e_x}$. Treating the transverse field $\boldsymbol{\delta B} = \theta B_0\boldsymbol{e_x}$ as a small magnetic perturbation, we get $\boldsymbol{\tau} = (V/\mu_0)\chi_\perp B_0^2\theta\boldsymbol{e_y}$. As expected, if $\chi_\perp$ is negative (positive), the torque tends to rotate the particle so that the NV center axis is aligned (perpendicular) to the magnetic field.

In our experiment, a 15 μm diameter diamond with a concentration of NV centers between 3–5 ppm is loaded in a 200 μm-diameter electrostatic trap with kHz angular frequencies (see Sec. II of the Supplemental Material [25]). The combined action of the Paul trap and magnetic torques $\boldsymbol{\tau}$ determines the angle of the four NV centers with respect to the external magnetic field. In order to characterize $\boldsymbol{\tau}$ and thus the NV-induced magnetism, we apply green laser light to polarize the NV centers in the $|m_s = 0\rangle$ state and sweep the frequency of a microwave signal at a power that is far from saturating the spin transition. At a spin resonance, a small magnetization is generated along $\boldsymbol{e_z}$, at which point the equilibrium angular position of the diamond is slightly modified. This mechanically detected-magnetic resonance technique (MDMR) [10] thus enables tracking of the angles of the four NV orientations with respect to the magnetic field $\boldsymbol{B}$. In order to measure $\boldsymbol{\tau}(\boldsymbol{B})$ and to probe the spin diamagnetism, we then run several scans under different magnetic field strengths (see Secs. III and VI of the Supplemental Material [25]).

One of the spectra is plotted in Fig. 1(b) for $B \approx 23$ mT, showing the characteristic opposite signals for $|0\rangle$ to $|\pm 1\rangle$ transitions of the same NV orientation [10]. Several other MDMR scans have been realized with B fields varying from 10 to 40 mT where we found that the extracted angles of the four NV orientations do not depend significantly on the applied magnetic field (see Sec. IV of the Supplemental Material [25]). The equilibrium angular position is thus largely determined by the electrostatic trap. A spectrum taken at $B \approx 180$ mT is shown in Fig. 1(c). Here, only two lines clearly detach from the spectrum with a very large signal to noise ratio. Importantly, their frequencies are consistent with an almost ideal alignment of one NV axis along the magnetic field. Such radically different spectra when $B \gtrapprox 105$ mT, are observed in almost all of the particles that we trap, pointing towards their microwave-free magneto-optical rotations.

A closer look to the $|m_s = 0\rangle$ to $|m_s = -1\rangle$ transition also confirms this hypothesis. The dashed line in the inset of Fig. 1(c) is a sketch of an asymmetrical MDMR in the weak microwave limit. When scanning a strong microwave tone the observed MDMR response instead features a slower increase on the red and a sharper decrease on the blue side. Such an asymmetrical mechanical response is the result of an interplay between the microwave sweep and the diamond rotation. When the microwave tone is red-detuned, the diamond rotates so that the energy difference between the $|0\rangle$ and $|-1\rangle$ states increases. During the scan, the NV resonance is dragged to the blue until the Paul trap restoring torque overcomes the magnetic torque, at which point the diamond rotates back to its equilibrium position. Populating the $|-1\rangle$ state thus misaligns the NV and magnetic fields axes. Therefore, the NV and magnetic fields are better aligned when the NV centers are the $|0\rangle$ state (see Sec. V of the Supplemental Material [25]).

Numerical calculations of the magnetic energy of the NV-doped diamond are shown in Sec. VII of the Supplemental Material [25]). The four [111] directions of the NV centers are seen to be strongly confining, with a potential depth that is 3 orders of magnitude larger than $kT \approx 10^{-21}$ J at $T = 300$ K, on the order of the Paul trap confinement. Beyond the GSLAC, the spins can thus efficiently pull the [111] crystalline direction towards the magnetic field direction, as expected for a diamagnetic anisotropic material.

In Fig. 2, the angle θ of the NV centers orientation that is closer to the magnetic field axis is measured experimentally as a function of the magnetic field amplitude (see Sec. IV of the Supplemental Material [25] for details about the angle calibration technique). Three regions can be identified.

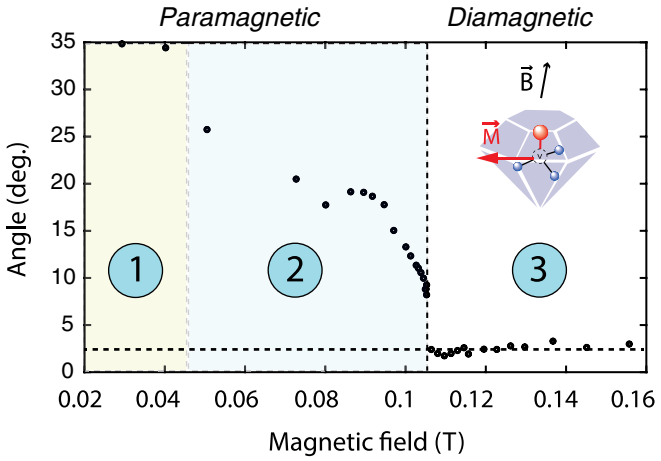

FIG. 2. Angle of one of the diamond [111] axes versus magnetic field amplitude.

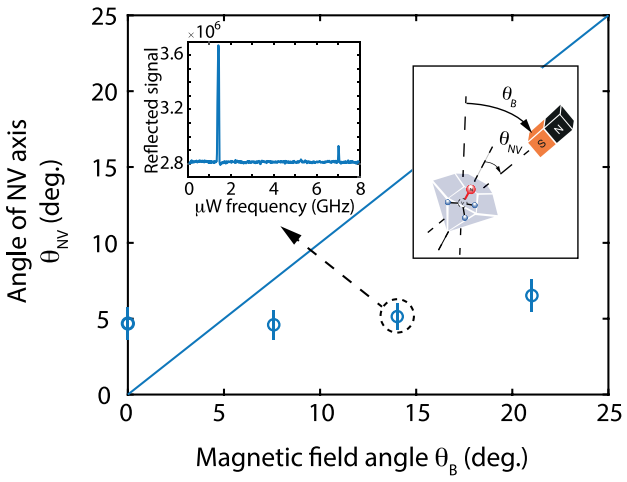

FIG. 3. Angle θ of the diamond [111] axis versus magnetic field angle θ_B (blue circles). See sketch in the inset on the top right. The plain blue line is the response that would be obtained without NV induced magnetism. The inset on the top left is a mechanically detected magnetic-resonance scan taken at $\theta_B \approx 14°$.

When the magnetic field ranges from 0 to 45 mT (region 1), θ does not change significantly. When the magnetic field increases from 45 to 105 mT however, θ reduces until it suddenly drops. The dependence of $\theta(B)$ in regions (1) and (2) results from a competition between the torque applied by the Paul trap and by the other three NV centers orientations (see Sec. IV of the Supplemental Material [25]). Importantly, close to 105 mT, a transition occurs where the angle between the NV centers and the magnetic field reaches ≈2°. The NV orientation remains locked to this value over a wide range of magnetic fields. The overall change of the NV angle is thus consistent with the above described transition from a paramagnetic state to a diamagnetic state at the ground state level anticrossing. The latter transition is expected to take place at $B_c = 102.4$ mT, which is very close to the observed critical B field ($B_c \approx 105$ mT). We explain this difference by the residual Paul trap torques which shift both θ and B_c (see Sec. VI of the Supplemental Material [25]). Another check that firmly establishes NV spin induced diamagnetism is that the particle [111] direction follows the magnetic field direction. This is demonstrated in Fig. 3 where, as the magnetic field direction is rotated, the angle between the NV and magnetic field axis departs from the linear law and remains at small angle values. Note that these are typical observations. Some diamonds with larger NV concentrations were even found to reach θ values that were less than a degree.

One of the striking features of the observed diamagnetism is its optical tunability. Figures 4(a) and 4(b) show that the NV axis can indeed be steered towards the magnetic field thanks to the laser induced polarization to the $|m_s = 0\rangle$ state. The magnetically induced librational frequency is also expected to increase with laser power once in the diamagnetic regime [region (3)]. Figures 4(c)(i) and 4(c)(ii) show the power spectral density (PSD) of the librational modes without (i) and with (ii) the green laser, showing a clear frequency shift of both librational modes (see Sec. VI of the Supplemental Material [25]). The increase of the observed librational frequencies with laser power is plotted in Fig. 4(d), showing again the strong magneto-optical nature of the effect. A study of its dependence with the magnetic field also shows the resonant boost of the librational

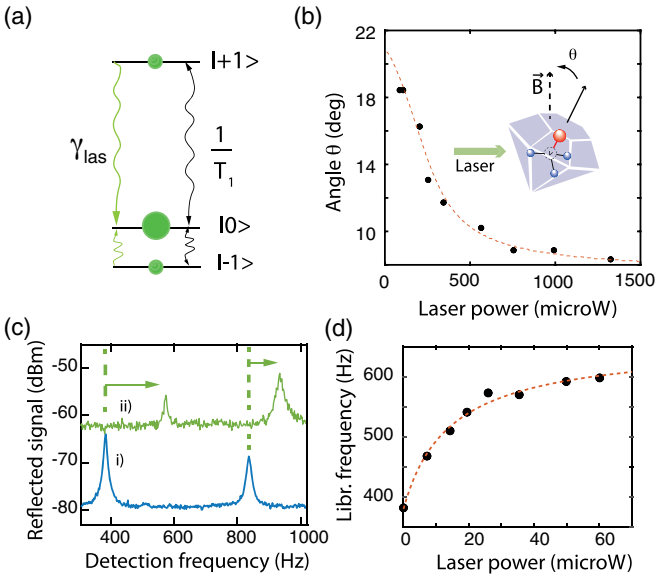

FIG. 4. a) NV center's electronic spin eigenstates in the $^3A_2$ state. Green arrows depicts the effective optical pumping to the $|m_s = 0\rangle$ state that results from the intersystem crossing in the optically excited ^3E state (not shown). Black arrows depict depolarizing mechanisms at rates $1/T_1$. b) Angle of one of the NV axes with respect to the magnetic field direction (as shown in the inset) as a function of the green laser power. c) Trace i) and trace ii), show the power spectral density of the librational modes without/with the green laser respectively. d) Librational frequency of the first mode as a function of laser power.

frequency close to the GSLAC (see Sec. VII of the Supplemental Material [25]).

Our observations open up several intriguing directions. First, the discovered diamagnetism should be strong enough to observe the diamagnetic *force* from the NV centers. Calculations even suggest that increasing the NV spin density by a factor of 10 and working with purer samples [31–33] will create an internal magnetization that is of the order of the applied magnetic field offering the prospect of using a diamond to expel magnetic field lines and thus to levitate them like in superconductor levitation.

Being able to align diamond main crystalline axes along magnetic fields also means that the embedded NVs can be easily employed for polarizing other species, such as the nuclear spins of the ^{13}C atoms of molecules under liquid environments [34–36]. Many groups are currently working towards polarizing paramagnetic species in solution using the NV centers inside nanodiamonds [5]. One difficulty with current attempts is to achieve large NV polarization under a fluctuating environment and under necessarily strong magnetic fields that are well-aligned to the NV axis. Our technique thus counteracts this drawback and may thus boost the hyperpolarization efficiency [37], opening a path towards more efficient NMR (see Sec. VII of the Supplemental Material).

More generally, our work may find applications for remote control of the motion of nano- or microscopic objects. As an example, the present magneto-optical confinement offers a solution for microwave-free stabilization of the angle of NDs in optical tweezers [16–18] with important perspectives for further spin-mechanical experiments in the quantum regime [14,38–41].

We would like to thank L. Rondin, V. Jacques, A. Dréau, and C. Voisin for fruitful discussions, as well as Ludovic Mayer for lending us microwave equipment. G. H. acknowledges science and engineering in Île-de-France region for quantum technologies (SIRTEQ) for funding.

[1] F. Casola, T. van der Sar, and A. Yacoby, Nat. Rev. Mater. **3**, 17088 (2018).
[2] D. D. Awschalom, R. Hanson, J. Wrachtrup, and B. B. Zhou, Nat. Photonics **12**, 516 (2018).
[3] L. P. McGuinness, Y. Yan, A. Stacey, D. A. Simpson, L. T. Hall, D. Maclaurin, S. Prawer, P. Mulvaney, J. Wrachtrup, F. Caruso, R. E. Scholten, and L. C. L. Hollenberg, Nat. Nanotechnol. **6**, 358 (2011).
[4] B. S. Miller, L. Bezinge, H. D. Gliddon, D. Huang, G. Dold, E. R. Gray, J. Heaney, P. J. Dobson, E. Nastouli, J. J. L. Morton, and R. A. McKendry, Nature (London) **587**, 588 (2020).
[5] D. E. J. Waddington, M. Sarracanie, H. Zhang, N. Salameh, D. R. Glenn, E. Rej, T. Gaebel, T. Boele, R. L. Walsworth, D. J. Reilly, and M. S. Rosen, Nat. Commun. **8**, 15118 (2017).
[6] X. Feng, W.-H. Leong, K. Xia, C.-F. Liu, G.-Q. Liu, T. Rendler, J. Wrachtrup, R.-B. Liu, and Q. Li, Nano Lett. **21**, 3393 (2021).
[7] R. Schirhagl, K. Chang, M. Loretz, and C. L. Degen, Annu. Rev. Phys. Chem. **65**, 83 (2014).
[8] M. Perdriat, C. Pellet-Mary, P. Huillery, L. Rondin, and G. Hétet, Micromachines **12**, 651 (2021).
[9] P. Rabl, P. Cappellaro, M. V. G. Dutt, L. Jiang, J. R. Maze, and M. D. Lukin, Phys. Rev. B **79**, 041302(R) (2009).
[10] T. Delord, P. Huillery, L. Nicolas, and G. Hétet, Nature (London) **580**, 56 (2020).
[11] J. S. Pedernales, G. W. Morley, and M. B. Plenio, Phys. Rev. Lett. **125**, 023602 (2020).
[12] Z. Yin, N. Zhao, and T. Li, Sci. China Phys. Mech. Astron. **58**, 1 (2015).
[13] M. Scala, M. S. Kim, G. W. Morley, P. F. Barker, and S. Bose, Phys. Rev. Lett. **111**, 180403 (2013).
[14] C. Wan, M. Scala, G. W. Morley, ATM. A. Rahman, H. Ulbricht, J. Bateman, P. F. Barker, S. Bose, and M. S. Kim, Phys. Rev. Lett. **117**, 143003 (2016).
[15] T. Delord, P. Huillery, L. Schwab, L. Nicolas, L. Lecordier, and G. Hétet, Phys. Rev. Lett. **121**, 053602 (2018).
[16] M. Geiselmann, M. L. Juan, J. Renger, J. M. Say, L. J. Brown, F. J. G. de Abajo, F. Koppens, and R. Quidant, Nat. Nanotechnol. **8**, 175 (2013).
[17] L. P. Neukirch, E. von Haartman, J. M. Rosenholm, and N. VamivakasA, Nat. Photonics **9**, 653 (2015).
[18] V. R. Horowitz, B. J. Alemn, D. J. Christle, A. N. Cleland, and D. D. Awschalom, Proc. Natl. Acad. Sci. U.S.A. **109**, 13493 (2012).
[19] J.-P. Tetienne, L. Rondin, P. Spinicelli, M. Chipaux, T. Debuisschert, J.-F. Roch, and V. Jacques, New J. Phys. **14**, 103033 (2012).
[20] J. H. Van Vleck, *The Theory of Electric and Magnetic Susceptibilities* (Clarendon Press, Oxford, 1932).
[21] R. L. Carlin, *Magnetochemistry* (Springer Science & Business Media, New York, 2012).
[22] M. W. Doherty, N. B. Manson, P. Delaney, F. Jelezko, J. Wrachtrup, and L. C. L. Hollenberg, Phys. Rep. **528**, 1 (2013).
[23] A. Abragam and B. Bleaney, *Electron Paramagnetic Resonance of Transition Ions* (Clarendon Press, Oxford, 1970).
[24] R. M. White, *Quantum Theory of Magnetism* (McGraw-Hill, New York, 1970).
[25] See Supplemental Material at http://link.aps.org/supplemental/10.1103/PhysRevLett.128.117203 for detail theoretical and experimental analyses, which includes Refs. [26–30].
[26] T. Delord, L. Nicolas, Y. Chassagneux, and G. Hétet, Phys. Rev. A **96**, 063810 (2017).
[27] P. Huillery, J. Leibold, T. Delord, L. Nicolas, J. Achard, A. Tallaire, and G. Hétet, Phys. Rev. B **103**, L140102 (2021).
[28] J. Choi, S. Choi, G. Kucsko, P. C. Maurer, B. J. Shields, H. Sumiya, S. Onoda, J. Isoya, E. Demler, F. Jelezko, N. Y. Yao, and M. D. Lukin, Phys. Rev. Lett. **118**, 093601 (2017), number: 9.
[29] C. Pellet-Mary, P. Huillery, M. Perdriat, and G. Hétet, Phys. Rev. B **104**, L100411 (2021).
[30] J. D. Breeze, E. Salvadori, J. Sathian, N. M. Alford, and C. W. M. Kay, Nature (London) **555**, 493 (2018).
[31] A. M. Edmonds *et al.*, arXiv:2004.01746.

[32] A. Tallaire, O. Brinza, P. Huillery, T. Delord, C. Pellet-Mary, R. Staacke, B. Abel, S. Pezzagna, J. Meijer, N. Touati, L. Binet, A. Ferrier, P. Goldner, G. Hetet, and J. Achard, Carbon **170**, 421 (2020).
[33] Y. Mindarava, R. Blinder, C. Laube, W. Knolle, B. Abel, C. Jentgens, J. Isoya, J. Scheuer, J. Lang, I. Schwartz, B. Naydenov, and F. Jelezko, Carbon **170**, 182 (2020).
[34] F. Shagieva, S. Zaiser, P. Neumann, D. B. R. Dasari, R. Stöhr, A. Denisenko, R. Reuter, C. A. Meriles, and J. Wrachtrup, Nano Lett. **18**, 3731 (2018).
[35] D. A. Broadway, J.-P. Tetienne, A. Stacey, J. D. A. Wood, D. A. Simpson, L. T. Hall, and L. C. L. Hollenberg, Nat. Commun. **9**, 1246 (2018).
[36] P. Fernández-Acebal, O. Rosolio, J. Scheuer, C. Müller, S. Müller, S. Schmitt, L. P. McGuinness, I. Schwarz, Q. Chen, A. Retzker, B. Naydenov, F. Jelezko, and M. B. Plenio, Nano Lett. **18**, 1882 (2018).
[37] J.-P. Tetienne, L. T. Hall, A. J. Healey, G. A. L. White, M.-A. Sani, F. Separovic, and L. C. L. Hollenberg, Phys. Rev. B **103**, 014434 (2021).
[38] C. Gonzalez-Ballestero, M. Aspelmeyer, L. Novotny, R. Quidant, and O. Romero-Isart, Science **374**, eabg3027 (2021).
[39] J. Millen, P. Z. G. Fonseca, T. Mavrogordatos, T. S. Monteiro, and P. F. Barker, Phys. Rev. Lett. **114**, 123602 (2015).
[40] Y. Ma, T. M. Hoang, M. Gong, T. Li, and Z.-q. Yin, Phys. Rev. A **96**, 023827 (2017).
[41] B.-B. Wei, C. Burk, and R.-B. Liu, Eur. Phys. J. Quantum Technol. **2**, 18 (2015).